

## Thermodynamic state-dependent structure-based coarse-graining of confined water

S. Y. Mashayak and N. R. Aluru

Citation: *J. Chem. Phys.* **137**, 214707 (2012); doi: 10.1063/1.4769297

View online: <http://dx.doi.org/10.1063/1.4769297>

View Table of Contents: <http://jcp.aip.org/resource/1/JCPSA6/v137/i21>

Published by the [American Institute of Physics](#).

---

### Additional information on *J. Chem. Phys.*

Journal Homepage: <http://jcp.aip.org/>

Journal Information: [http://jcp.aip.org/about/about\\_the\\_journal](http://jcp.aip.org/about/about_the_journal)

Top downloads: [http://jcp.aip.org/features/most\\_downloaded](http://jcp.aip.org/features/most_downloaded)

Information for Authors: <http://jcp.aip.org/authors>

## ADVERTISEMENT



**Goodfellow**  
metals • ceramics • polymers • composites  
70,000 products  
450 different materials  
**small quantities fast**

[www.goodfellowusa.com](http://www.goodfellowusa.com)

# Thermodynamic state-dependent structure-based coarse-graining of confined water

S. Y. Mashayak and N. R. Aluru<sup>a)</sup>

Department of Mechanical Science and Engineering, Beckman Institute for Advanced Science and Technology, University of Illinois at Urbana-Champaign, Urbana, Illinois, 61801, USA

(Received 6 September 2012; accepted 15 November 2012; published online 7 December 2012)

We develop thermodynamic state-dependent single-site isotropic coarse-grained potentials to predict the structure of water confined inside graphene slit-like channels by two multiscale simulation approaches: the coarse-grained molecular dynamics (CG-MD) and the empirical potential-based quasi-continuum theory (EQT). The structurally-consistent coarse-grained potentials for the CG-MD and EQT are systematically determined from the reference all-atom SPC/E water MD (AA-MD) results. For optimization of the CG-MD potentials, the relative entropy based coarse-graining method is used, and for determination of the EQT potentials, we develop a potential of mean force matching scheme. The optimized coarse-grained potentials are found to be dependent on the thermodynamic state. They are evaluated for their ability to predict the density profile of confined water, and it is found that the results obtained by the CG-MD and EQT simulations are in good agreement with the reference AA-MD results. © 2012 American Institute of Physics. [<http://dx.doi.org/10.1063/1.4769297>]

## I. INTRODUCTION

Water in confined spaces, especially at length scales ranging from a few Angstroms to several nanometers, exhibits highly unusual properties.<sup>1</sup> Study of these unusual properties of confined water is important to understand the function of biomolecular systems and enables the design of novel nanofluidic applications.<sup>2</sup> Nanoscale structure and properties of water cannot be captured by the classical continuum models.<sup>3</sup> Therefore, over the past decade, molecular simulation techniques, such as molecular dynamics (MD) and Monte Carlo (MC) simulations, have been widely used to study the microscopic properties of confined water. However, these techniques are computationally expensive, and accessible time and length scales are limited. As a result, these methods are not applicable for many applications of practical interest that involve multiple time and length scales ranging from the quantum to atomic to continuum scales.<sup>4</sup>

Recently, various multiscale simulation approaches have been developed to efficiently simulate systems of multiple time and length scales.<sup>4-6</sup> Based on the resolution level, various simulation approaches can be divided into four main categories: (i) quantum level, which is the fundamental level where the change in electronic wavefunctions are explicitly considered, (ii) detailed all-atom (AA) level, where the electrons are considered only implicitly but all the atoms of the given system are explicitly simulated, (iii) intermediate particle-based coarse-grained (CG) level, where several atoms of the given system are represented by a single CG bead, and (iv) continuum level where the system is represented by volume elements such as in computational fluid dynamics. Multiscale simulation methods try to capture properties of a given system at various levels of resolution by combining and/or

linking different simulation models. It is important that the individual models on different levels of resolution are systematically linked such that these models are thermodynamically and/or structurally consistent. This scale-bridging can be achieved by appropriately devising the effective interaction potentials at different levels of resolution. The process of determining effective interactions at coarser-level from more detailed high resolution level is referred to as the systematic coarse-graining.

The objective of this study is to systematically coarse-grain degrees of freedom of confined water from the detailed all-atom level to the cheaper particle-based CG level, and to the continuum-based level. There exists many different AA level models for water with varied degrees of complexity and accuracy.<sup>7,8</sup> Here, we use the extended simple point charge (SPC/E)<sup>9</sup> model for the AA level confined water simulations. Though particle-based CG systems are simulated using similar molecular simulation techniques as in AA simulations, they allow faster computations due to reduced degrees of freedom and simpler interaction potentials as compared to AA models. For continuum-based simulation, we use empirical potential-based quasi-continuum theory (EQT).<sup>10</sup> EQT is a simple and fast approach to predict the inhomogeneous density and potential profiles of a confined fluid. In EQT, for a slit-channel system, the 1-D steady-state Nernst-Planck (NP) equation,

$$\frac{d}{dz} \left( \frac{d\rho}{dz} + \frac{\rho}{RT} \frac{dU}{dz} \right) = 0, \quad (1)$$

with boundary conditions

$$\rho(0) = 0, \quad (2a)$$

$$\rho(L) = 0, \quad (2b)$$

<sup>a)</sup>Electronic mail: aluru@illinois.edu.

$$\frac{1}{L} \int_0^L \rho(z) dz = \rho_{avg}, \quad (2c)$$

is solved to obtain self-consistent density and potential profiles of a confined fluid. In Eqs. (1) and (2),  $\rho$  is the fluid density,  $U$  is the total potential,  $T$  is the fluid temperature,  $R$  is the ideal gas constant,  $L$  is the channel width,  $\rho_{avg}$  is the average density of confined fluid, and  $z$  is the direction perpendicular to the slit-channel wall. The principal idea in EQT is to compute  $U$  by the continuum approximation. In the continuum approximation, wall and fluid particles are represented by their local densities, and  $U$  is determined by separately summing the contributions from the wall and fluid as a density weighted integration of the effective quasi-continuum interaction potentials over the surrounding medium, i.e.,

$$U(r) = \int \rho_{wall}(r') u^{wf}(|r - r'|) dr' + \int \rho(r') u^{ff}(|r - r'|) dr', \quad (3)$$

where  $\rho_{wall}$  is the wall atom density,  $u^{wf}(r)$  and  $u^{ff}(r)$  are the effective wall-fluid and fluid-fluid quasi-continuum pair potentials, respectively. Further details on EQT can be found in Refs. 10 and 11.

Various systematic coarse-graining methods have been developed to derive thermodynamically and/or structurally consistent CG potentials, such as iterative Boltzmann inversion (IBI), inverse Monte Carlo (IMC), force matching (FM), and relative entropy minimization.<sup>12-14</sup> In the literature, these methods have been used to develop CG potentials for bulk water, which can reproduce structural properties such as the radial distribution function (RDF).<sup>13-15</sup> However, the structure of confined water can be very different from bulk water,<sup>1</sup> hence, CG potentials for bulk water cannot reproduce the structural properties of confined water. In Ref. 11, we developed CG potential models for the structural prediction of water confined inside graphite and silicon slit-like channels at the standard thermodynamic state. CG models, however, suffer from transferability issues, i.e., they are thermodynamic state dependent and may not be accurate for states other than the reference state for which they are optimized.<sup>16,17</sup> Therefore, the focus of this study is to develop thermodynamic state dependent CG potentials of confined water for the particle-based CG and EQT simulation approaches.

The remainder of the paper is organized as follows. In Sec. II, we provide the reference MD simulation details of the confined water systems considered. In Sec. III, we describe the functional forms and coarse-graining techniques used to model the CG potentials. Accuracy and transferability of these CG potentials are discussed in Sec. IV. Finally, we draw conclusions in Sec. V.

## II. MD SIMULATIONS

We simulate water structure between two flat parallel graphene layers at various thermodynamic states, from ambient (298 K) to supercritical conditions (673 K) with a range of densities between 0.66 and 1.0 g/cm<sup>3</sup> simi-

lar to the one considered in Ref. 18. The two graphene layers are placed along the XY plane, and the lateral dimensions of the layers are 3.83400 × 3.68927 nm<sup>2</sup>. The  $z$  coordinate is perpendicular to the graphene layers, and the separation distance between the two graphene layers is varied from  $2\sigma$  to  $20\sigma$ , where  $\sigma$  (=0.317 nm) is the length-scale parameter for the Lennard-Jones interaction between oxygen atoms of water molecules. We follow the same procedure described in Ref. 11 to determine the average density,  $\rho_{avg}$ , of confined water, which is defined as  $\rho_{avg} = \text{no. of molecules adsorbed/volume of the channel}$ . For channels of widths larger than  $4\sigma$ , linear superposition approximation (LSA)<sup>19</sup> is used to determine  $\rho_{avg}$ , and for smaller channels, isothermal-isosurface-isobaric ensemble<sup>20</sup> equilibration simulations are performed with the channel attached to the bulk water reservoir at the saturated liquid density for the corresponding temperature and saturation pressure, which are obtained from Ref. 21.

All-atom molecular dynamic (AA-MD) simulations are performed in the NVT (canonical) ensemble by GROMACS.<sup>22</sup> Water is modeled using the extended simple point charge (SPC/E)<sup>9</sup> model; the interaction parameters are the same as in Ref. 11. Spherical cutoff of 1.5 nm is used for the Lennard-Jones interactions, and electrostatic interactions are computed by the particle mesh Ewald (PME)<sup>23</sup> method with an extra vacuum of 19 nm above the graphene layer along with the appropriate correction for the slab geometry. Wall atoms are kept fixed at their original positions. Periodic boundary conditions are specified in the  $x$ ,  $y$ , and  $z$  directions. Temperature is maintained using the Nosé-Hoover thermostat<sup>24</sup> with 0.2 ps time constant. All systems are equilibrated for 5 ns and production runs of 45 ns are performed with 1 fs time step. The density profiles are computed using 0.05 $\sigma$  bin size along the  $z$  direction.

We also perform coarse-grained MD (CG-MD) simulations using the CG potentials developed in this work. CG-MD simulations are performed using GROMACS with the same system settings as for the AA-MD simulations, except that the CG interactions are specified using the tabulated potentials. With 1 fs timestep, it is found that the CG-MD simulations are 5 times faster than the AA-MD simulations.

## III. STRUCTURE-BASED COARSE-GRAINING

It is often the case that the models with coarse-grained interactions cannot reproduce simultaneously all the thermodynamic and structural properties of the reference system.<sup>15-17</sup> Here, the property of interest for coarse-graining is the equilibrium center of mass (COM) density profile of confined water obtained by the reference AA-MD simulations at various thermodynamic states and channel widths. We follow the approach in which first the coarse-grained interactions for the CG-MD are determined from the reference AA-MD results and then the effective interactions for the EQT are optimized. Methods we use to determine such effective interactions for the CG-MD and EQT approaches are discussed in Subsections III A and III B.

## A. CG-MD potentials

In the CG-MD model for the confined water system, we represent one water molecule with one coarse-grained bead at the COM and retain all the atomistic details of the graphene layers. In this representation of the confined water system, we need to specify the effective interaction potentials between water-water CG beads and between graphene-water CG beads. In the reference all-atom model, carbon atoms of the graphene layers are modeled as simple LJ-type atoms, and hence, the interaction between a carbon atom and a water molecule is already a single-site isotropic potential. However, as discussed in Ref. 11, due to inherent inhomogeneity of the confined water micro-structure, a single spatially uniform water-water CG pair potential along with the original wall-water LJ pair potential may not reproduce the structural properties of confined water. To address this issue, in Ref. 11, we used the coarse-grained correction potential between a wall atom and a water CG bead in addition to the original LJ potential. Here, instead of separately modeling these two types of CG potentials between a wall atom and a water CG bead, we consider a single effective carbon-water CG potential, and optimize it such that it accounts for the surface effects on the water structure.

To model the water-water CG-MD potential,  $u_{CG}^{ww}(r)$ , and the carbon-water CG-MD potential,  $u_{CG}^{cw}(r)$ , we use a functional form based on uniform cubic B-splines (SP). In a pair potential function,  $u_{SP}(r)$ , based on uniform cubic B-splines, the separation interval from 0 to the cut-off distance,  $R_{cut}$ , is discretized into  $n - 1$  segments,  $\{r_0, r_1, r_2, \dots, r_{n-1}\}$ , of equal size  $\Delta r = R_{cut}/(n - 1)$  such that  $r_i = i \times \Delta r$ , where  $i \in (0 \dots n - 1)$ . Then, given  $n + 2$  real values  $\{c_0, c_1, c_2, \dots, c_{n+1}\}$  called the spline knots, the value of a pair potential at a separation distance  $r$  is determined by

$$u_{SP}(r) = [1 \quad t \quad t^2 \quad t^3] \frac{1}{6} \begin{bmatrix} 1 & 4 & 1 & 0 \\ -3 & 0 & 3 & 0 \\ 3 & -6 & 3 & 0 \\ -1 & 3 & -3 & 1 \end{bmatrix} \begin{bmatrix} c_j \\ c_{j+1} \\ c_{j+2} \\ c_{j+3} \end{bmatrix}, \quad (4)$$

where the index  $j$  is determined such that  $r_j \leq r < r_{j+1}$ , and  $t$  is given by

$$t = \frac{r - r_j}{\Delta r}. \quad (5)$$

The SP potential form,  $u_{SP}(r)$ , is not only suitable for analytical treatment, but also exhibits remarkable flexibility and can represent various complex functional characteristics of pair potentials for sufficiently large number of knots. In this work, for both  $u_{CG}^{ww}(r)$  and  $u_{CG}^{cw}(r)$ , we set  $R_{cut} = 1.0$  nm with a grid spacing of  $\Delta r = 0.02$  nm, i.e.,  $n = 51$ . Thus, we need to optimize a total of 53 knot values for each CG-MD potential, i.e., the knot values  $\{c_{0,CG}^{ww}, c_{1,CG}^{ww}, c_{2,CG}^{ww}, \dots, c_{52,CG}^{ww}\}$  for the water-water CG-MD potential and the knot values  $\{c_{0,CG}^{cw}, c_{1,CG}^{cw}, c_{2,CG}^{cw}, \dots, c_{52,CG}^{cw}\}$  for the carbon-water CG-MD potential.

To determine the optimum spline knots for  $u_{CG}^{ww}(r)$  and  $u_{CG}^{cw}(r)$ , we use the recently introduced coarse-graining method by Shell<sup>25</sup> based on the relative entropy,  $S_{rel}$ , defined

as

$$S_{rel} = \sum_i p_{AA}(i) \ln \left( \frac{p_{AA}(i)}{p_{CG}(M(i))} \right) + \langle S_{map} \rangle_{AA}, \quad (6)$$

where  $i$  is a particular configuration of the atom sites in the AA-MD ensemble,  $M$  is the mapping operation to generate a corresponding configuration  $I$  of the CG sites, i.e.,  $I = M(i)$ ,  $p_{AA}$  and  $p_{CG}$  are the configurational probabilities based on the AA-MD and CG-MD potentials, respectively, and  $\langle S_{map} \rangle_{AA}$  is the mapping entropy due to the average degeneracy of the AA configurations mapping to the same CG configuration, given by

$$S_{map}(I) = \ln \sum_i \delta_{I,M(i)}, \quad (7)$$

where  $\delta$  is the Kronecker delta function. From Eq. (7), it can be shown that  $\langle S_{map} \rangle_{AA}$  does not depend on the CG-MD potential parameters, but it is a unique function of the mapping operator,  $M$ , and the AA configurational probabilities,  $p_{AA}(i)$ . The log-likelihood based derivation of the relative entropy for molecular systems, as defined in Eq. (6), is provided in Ref. 25. The relative entropy quantifies the extent of the configurational phase-space overlap between two molecular ensembles.<sup>26</sup> It is a measure of the discrepancies between various properties of the CG-MD and AA-MD ensembles. Physically,  $S_{rel}$  can be interpreted as the log-probability that one test configuration of the model CG-MD ensemble is representative of the target AA-MD ensemble, and when the likelihood is a maximum,  $S_{rel}$  is at a minimum. Hence, the numerical minimization of  $S_{rel}$  with respect to the parameters of the CG-MD model can be used to optimize it. One of the advantages of the relative entropy based coarse-graining is that one can design CG potentials using analytical function forms, which are desired in the theoretical treatments such as EQT, whereas, methods, such as IBI, use tabulated potentials. Also, Chaimovich and Shell<sup>27</sup> have demonstrated that there exist connections between the relative entropy based coarse-graining method and other coarse-graining methods. In Ref. 27, it was shown that under some conditions based on the modeling of CG potentials, relative entropy minimization can give the same CG potentials as other methods, e.g., it is equivalent to the IBI when the CG interactions are modeled using the finely tabulated pair additive potentials, and to the FM when the CG potential is modeled in the most general way such that it is a function in the space of  $N$ -body interactions, where  $N$  is the number of coarse-grained degrees of freedom. More details about the relative entropy based coarse-graining method and its applications can be found in Refs. 14, 25, 27, and 28. As described in Sec. II, both the AA-MD and CG-MD systems are considered in the canonical ensemble. In the canonical ensemble, the relative entropy simplifies to

$$S_{rel} = \beta \langle U_{CG} - U_{AA} \rangle_{AA} - \beta \langle A_{CG} - A_{AA} \rangle_{AA} + \langle S_{map} \rangle_{AA}, \quad (8)$$

where all the averages are computed in the reference AA-MD ensemble, and  $A_{CG}$  and  $A_{AA}$  are the configurational part of the Helmholtz free energies from the CG-MD and the AA-MD potentials, respectively.

The CG-MD potential parameters,  $\lambda = \{c_{0,CG}^{ww}, c_{1,CG}^{ww}, c_{2,CG}^{ww}, \dots, c_{52,CG}^{ww}, c_{0,CG}^{cw}, c_{1,CG}^{cw}, c_{2,CG}^{cw}, \dots, c_{52,CG}^{cw}\}$ , are optimized by minimizing  $S_{rel}$ . Here, we follow the coupled Newton-Raphson strategy for the relative entropy minimization as described in Ref. 27. In this approach, the parameters  $\lambda$  are refined iteratively as

$$\lambda^{k+1} = \lambda^k - \chi \mathbf{H}_{S_{rel}}^{-1} \cdot \nabla_{\lambda} S_{rel}, \quad (9)$$

where  $k$  is the iteration index,  $\chi \in (0 \dots 1)$  is the relaxation parameter that can be adjusted to ensure the convergence,  $\nabla_{\lambda} S_{rel}$  is the vector of the first derivatives of  $S_{rel}$  with respect to  $\lambda$  and  $\mathbf{H}_{S_{rel}}$  is the Hessian matrix of  $S_{rel}$ . The details of computing  $S_{rel}$  and  $\mathbf{H}_{S_{rel}}$  are given in Appendix A. This procedure of optimizing the CG-MD potential parameters by the relative entropy minimization is implemented in the open-source VOTCA code,<sup>12</sup> and it will be available in version 1.3 of VOTCA. The optimized carbon-water and water-water CG-MD potentials obtained by the relative entropy minimization are discussed in Subsection IV A.

## B. EQT potentials

As described in Sec. I, in EQT, we need the effective carbon-water and water-water quasi-continuum pair poten-

tials to evaluate the total potential profile,  $U(z)$ , by Eq. (3). In prior works,<sup>10,11,29,30</sup> it was shown that one can use the particle-based effective single-site isotropic pair potential between a wall particle and a fluid particle to determine the wall-fluid contribution to  $U(z)$ . Thus, to compute the carbon-water potential profile,  $U^{cw}(z)$ , we use the CG-MD carbon-water pair potential as

$$U^{cw}(r) = \int \rho_c(r') u_{CG}^{cw}(|r - r'|) dr', \quad (10)$$

where,  $\rho_c$  is the density of carbon atoms in the graphene layer, which is taken to be 38.18 atoms/nm<sup>2</sup>. The fluid-fluid part, i.e., the water-water potential profile,  $U^{ww}(z)$ , is given by

$$U^{ww}(r) = \int \rho(r') u_{EQT}^{ww}(|r - r'|) dr', \quad (11)$$

where  $u_{EQT}^{ww}(r)$  is the water-water effective quasi-continuum pair potential. One should model  $u_{EQT}^{ww}(r)$ , such that it is finite for  $r \rightarrow 0$ , and it should take into account the effects of the neglected pair correlations in the mean-field approximation (MFA) of Eq. (11).<sup>11</sup> Therefore, we model the water-water effective quasi-continuum pair potential,  $u_{EQT}^{ww}(r)$ , as

$$u_{EQT}^{ww}(r) = \begin{cases} 0, & r \leq R_{crit} \\ a_0 + a_1(r - R_{min}) + a_2(r - R_{min})^2, & R_{crit} < r \leq R_{min}, \\ u_{SP}(r), & R_{min} < r \leq R_{cut} \end{cases} \quad (12)$$

where  $R_{crit}$  and  $R_{min}$  are the control parameters, which define the zero potential region and the soft-core of  $u_{EQT}^{ww}(r)$ , respectively. The soft-core region is modeled using the quadratic polynomial with the coefficients  $a_0$ ,  $a_1$ , and  $a_2$ . Similar approach of modeling the soft-core of the fluid-fluid quasi-continuum pair potentials to ensure the finite potential values for small  $r$  is followed previously in Refs. 10, 11, 29, and 30. In the region from  $R_{min}$  to the cut-off distance  $R_{cut}$ ,  $u_{EQT}^{ww}(r)$  is modeled using the uniform cubic B-splines form,  $u_{SP}(r)$ , given by Eq. (4). In this work, we optimize  $a_1$ ,  $a_2$ , and the cubic B-spline knot values of  $u_{EQT}^{ww}(r)$  in Eq. (12), i.e.,  $\lambda = \{a_1, a_2, c_{0,EQT}^{ww}, c_{1,EQT}^{ww}, c_{2,EQT}^{ww}, \dots\}$ . We fix  $R_{crit} = 0.05$  nm,  $R_{min} = 0.26$  nm,  $R_{cut} = 1.04$  nm, and use grid spacing of 0.08 nm for the cubic B-spline part of  $u_{EQT}^{ww}(r)$ .  $a_0$  is determined by imposing the  $C^0$  continuity condition at  $R_{min}$ .

Here, we develop a systematic technique to optimize the parameters  $\lambda$  of  $u_{EQT}^{ww}(r)$  such that the target equilibrium COM density profile,  $\rho^{tgt}(z)$ , of the confined water can be reproduced by EQT. Similar to the IBI method, in which, to reproduce the target RDF, the CG potential is optimized such that the Boltzmann relation between the two-body PMF and the RDF is satisfied, for reproducing  $\rho^{tgt}(z)$  the parameters of  $u_{EQT}^{ww}(r)$  must satisfy the Boltzmann relation

given by

$$\rho(z) = \rho_0 \exp\left(-\frac{\bar{U}(z)}{RT}\right), \quad (13)$$

where  $\rho_0$  is the density at the reference point  $z_0$  and  $\bar{U}(z)$  is the total PMF profile computed as

$$\bar{U}(z) = U(z) - U(z_0). \quad (14)$$

Here, for the slit-like graphene-water system, we use the midpoint of the channel as the reference point. Therefore, to quantify the accuracy of  $u_{EQT}^{ww}(r)$  parameters, we define the metric:

$$\epsilon_B = \frac{1}{2L} \int_0^L \left( \rho_0^{tgt} \exp\left(-\frac{\bar{U}(z)}{RT}\right) - \rho^{tgt}(z) \right)^2 dz, \quad (15)$$

where  $\rho_0^{tgt}$  is the target density at the reference point  $z_0$  and  $\bar{U}(z)$  is determined by using the target density profile,  $\rho^{tgt}(z)$ . The quantity  $\epsilon_B$  in Eq. (15) gives the average squared error in the Boltzmann relation due to the given parameters of  $u_{EQT}^{ww}(r)$ . Hence, the objective is to determine the parameters of  $u_{EQT}^{ww}(r)$  such that the quantity  $\epsilon_B$  is minimized. Since, minimizing  $\epsilon_B$  is equivalent to reproducing the target total PMF profile, it is in essence a PMF-matching technique.

Similar to the relative entropy minimization as described in Subsection III A, for the minimization of  $\epsilon_B$ , we use the coupled Newton-Raphson scheme such that the parameters of  $u_{\text{EQT}}^{\text{ww}}(r)$ ,  $\lambda$ , are refined iteratively as

$$\lambda^{k+1} = \lambda^k - \chi \mathbf{H}_{\epsilon_B}^{-1} \cdot \nabla_{\lambda} \epsilon_B, \quad (16)$$

where  $k$  and  $\chi$  have the same definitions as in Eq. (9),  $\nabla_{\lambda} \epsilon_B$  is the vector of the first derivatives of  $\epsilon_B$  with respect to  $\lambda$ , and  $\mathbf{H}_{\epsilon_B}$  is the Hessian matrix of  $\epsilon_B$ . The details of computing  $\nabla_{\lambda} \epsilon_B$  and  $\mathbf{H}_{\epsilon_B}$  are given in Appendix B. More discussion on the values of  $R_{\text{crit}}$ ,  $R_{\text{min}}$ , and the optimized EQT potentials is given in Subsection IV B.

## IV. RESULTS

The COM density profiles of water confined inside the graphene channel for a range of channel widths at different thermodynamic states obtained from the reference AA-MD simulations are illustrated in Fig. 2. It can be seen that at all thermodynamic states and channel widths, there exist two distinguishable water layers near the graphene surface. For channels larger than  $6\sigma$ , beyond the second interfacial layer, there exists bulklike water in the central region of a channel. The locations of both the interfacial layers do not vary much with the thermodynamic state, i.e., the first and second layers are located near  $1.025\sigma$  and  $1.956\sigma$ , respectively, from the graphene surface at all thermodynamic states. Whereas, the relative magnitudes of the interfacial density layers decrease with decrease in  $\rho_{\text{bulk}}$ . Similar observations about the thermodynamic state dependence of density profile of water confined inside the graphene channel are made by Martí and Guàrdia.<sup>18</sup>

Since the average contributions of the coarse-grained atomic degrees of freedom depend on the thermodynamic state of the reference system, CG potentials suffer from transferability issues, i.e., CG potential constructed from a reference system at a given thermodynamic state may not directly be used for modeling the underlying system at a different state point.<sup>16,17</sup> Therefore, we generate a different set of CG-MD and EQT potentials for each thermodynamic state of the confined water, given in Table I. For both, the relative entropy minimization and the PMF-matching based coarse-graining, we use the  $10\sigma$  channel AA-MD system as the target system. We find that, as described in Subsections IV A and IV B, though the CG potentials are optimized for the reference  $10\sigma$  channel of each thermodynamic state, they are transferable across different channel widths at the same thermodynamic state.

TABLE I. Thermodynamic states of confined water considered in this work.

State	T [K]	$\rho$ [gm/cm <sup>3</sup> ]
I	298	1.0
II	328	0.985
III	400	0.935
IV	523	0.8
V	673	0.66

## A. CG-MD potentials

Fig. 1 shows the carbon-water and water-water CG-MD potentials obtained by the relative entropy minimization for different thermodynamic states. The optimum parameter values of the CG-MD potentials are provided in the supplementary information.<sup>31</sup> We first evaluate these CG-MD potentials for their ability to predict the COM density profile of the confined water by performing the CG-MD simulations. Fig. 2 shows the CG-MD results for the COM density profiles of water in multiple channel widths at different thermodynamic states. It is evident that the CG-MD potentials predict the COM density profile of the confined water sufficiently accurately as compared to the reference AA-MD results, and it is found that the root-mean-squared deviation (RMSD) between the CG-MD and AA-MD results is less than 0.055.

From Fig. 1, further observations can be made about the state dependent characteristics of the water-water and carbon-water CG-MD potentials. It can be seen that both the CG-MD pair potentials depend substantially on the thermodynamic state. However, water-water CG-MD potential exhibits a characteristic core-softened double-well-type form at all the states considered. This observation is consistent with the studies of single-site isotropic potentials for water.<sup>13,14,17,32,33</sup> There are two important energy and length-scales to core-softened double-well-type potential form. We find that, for the water-water CG-MD potential, the energy-scale of the first well varies significantly with the thermodynamic state: it

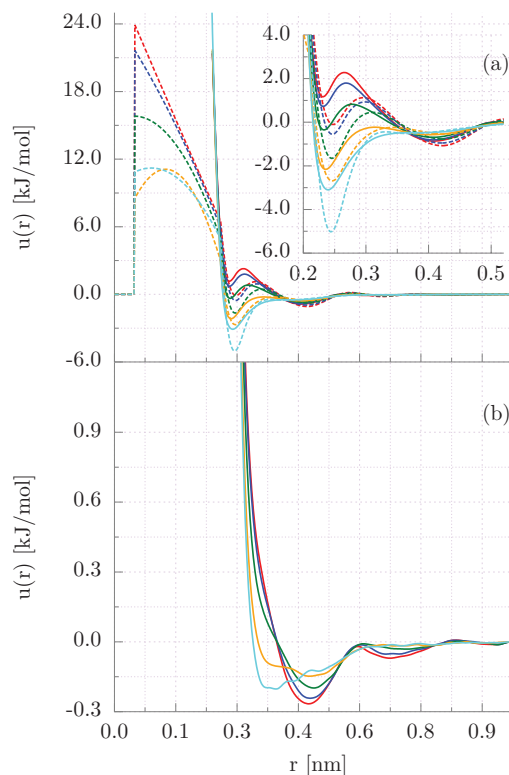


FIG. 1. Coarse-grained effective potentials for CG-MD and EQT simulations at different thermodynamic states. The top subfigure shows water-water potentials where solid lines are CG-MD potentials and dashed lines are EQT potentials. The bottom subfigure shows carbon-water potentials. In both the subfigures, red lines are for  $T = 298$  K, blue for  $T = 328$  K, green for  $T = 400$  K, orange for  $T = 523$  K, and cyan for  $T = 673$  K.

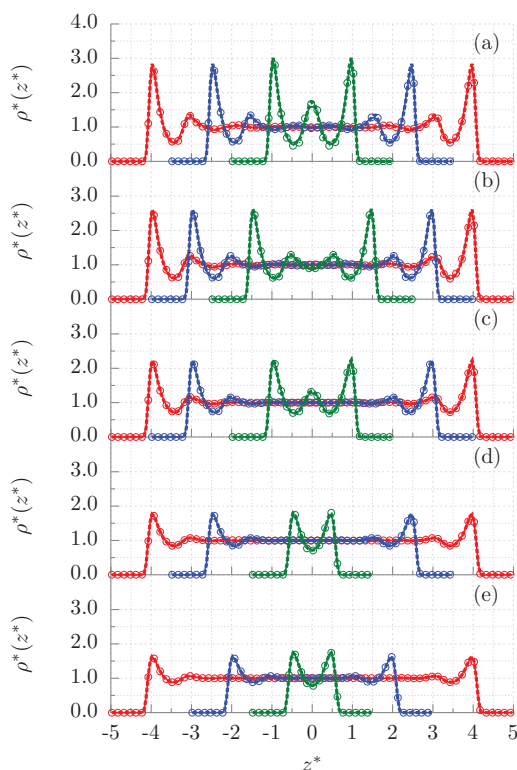


FIG. 2. Comparison of COM density profiles of water from AA-MD, CG-MD, and EQT simulations at different thermodynamic states and channel widths: (a)  $T = 298$  K,  $10\sigma$  (red),  $7\sigma$  (blue), and  $4\sigma$  (green); (b)  $T = 328$  K,  $10\sigma$  (red),  $8\sigma$  (blue), and  $5\sigma$  (green); (c)  $T = 400$  K,  $10\sigma$  (red),  $8\sigma$  (blue), and  $4\sigma$  (green); (d)  $T = 523$  K,  $10\sigma$  (red),  $7\sigma$  (blue), and  $3\sigma$  (green); and (e)  $T = 673$  K,  $10\sigma$  (red),  $6\sigma$  (blue), and  $3\sigma$  (green). In all subfigures, circles are AA-MD results, solid lines are CG-MD results, and dashed lines are EQT results.  $z^*$  is defined as  $z/\sigma$  and  $\rho^* = \rho/\rho_{\text{bulk}}$ ; value of  $\rho_{\text{bulk}}$  for each  $T$  is given in Table I.

continuously falls from positive values at lower temperatures to negative values at higher temperatures. The second-well is always attractive and does not vary significantly with the thermodynamic state. Also, we note that the difference between the second inflection point and the second energy well decreases with increasing temperature. Wang *et al.*<sup>15</sup> suggest that this difference governs the tetrahedral packing of water molecules: the larger the difference, the stronger the tetrahedral packing. This implies that for the graphene-water system as temperature increases the tetrahedral packing of water molecules becomes weaker, which is physically consistent with the observations by Martí and Guàrdia<sup>18</sup> that as temperature increases, the number of hydrogen bonds per water molecule decreases. In contrast to the significant state dependence of the energy-scales, both the length-scales, i.e., locations of the first and second well, vary very little with the state, and the ratio of the two length-scales is in the range 0.61–0.67, which is in agreement with the observation made by Yan *et al.*,<sup>32</sup> that in order to have water-like characteristics, this ratio should be  $\approx 0.6$ . Similar observations are made by Chaimovich and Shell<sup>14</sup> about the thermodynamic state dependence of the energy and length-scales of the coarse-grained bulk water potential.

## B. EQT potentials

As mentioned in Subsection III B, in EQT, we use the same CG-MD potential for the carbon-water pair interaction. Fig. 1 shows the optimum water-water pair potentials for EQT obtained by the PMF-matching method. The optimum parameter values of  $u_{\text{EQT}}^{\text{ww}}(r)$  are provided in the supplementary information.<sup>31</sup> We note that, for each thermodynamic state, the optimum values of  $a_1, a_2$ , and the cubic B-spline knot values for  $u_{\text{EQT}}^{\text{ww}}(r)$  depend significantly on the choice of  $R_{\text{crit}}$  and  $R_{\text{min}}$  values. Herein, we set  $R_{\text{crit}} = 0.05$  nm and  $R_{\text{min}} = 0.26$  nm for all the thermodynamic states such that the optimized  $u_{\text{EQT}}^{\text{ww}}(r)$  follows as closely as possible the characteristics of the CG-MD water-water potential in the region from  $R_{\text{min}}$  to  $R_{\text{cut}}$ . As discussed in Subsection III B, the soft-core part of the  $u_{\text{EQT}}^{\text{ww}}(r)$  for the region  $r < R_{\text{min}}$  has mainly been introduced to avoid the numerical singularity issues, and it lacks any physical justification. It can be observed that, for each thermodynamic state, though the water-water EQT potential has the same core-softened double-well-type characteristics as in the CG-MD case, its length-scales are slightly shifted and energy-scales are more attractive as compared to the CG-MD water-water potential. This behaviour can be contributed to the MFA of Eq. (11).<sup>34</sup> The MFA neglects the water-water pair correlations, which should enhance the attractive interactions. Hence, the effective water-water EQT potentials are more attractive to account for the effects of the pair correlation.

Next, we evaluate these EQT potentials for their ability to predict the COM density profile of the confined water by performing the EQT simulations. As described in Ref. 10, the numerical algorithm based on an iterative scheme is used to solve Eqs. (1), (2), (3), (10) and (11) in a self-consistent manner. From Fig. 2, it is evident that the EQT potentials predict the COM density profile of the confined water accurately as compared to the reference AA-MD results, and it is found that the RMSD between the EQT and AA-MD results is less than 0.044.

## C. Transferability

Although, the CG potentials are significantly state-dependent, one can transfer a CG potential optimized for a particular thermodynamic state to a different state by an appropriate state-dependent scaling relation.<sup>35</sup> Such scaling relations, if exist, can be useful to derive CG potentials for wider thermodynamic states from the CG potentials of a few representative states, which are optimized explicitly by a coarse-graining technique. Farah *et al.*<sup>35</sup> used a 2-point linear interpolation formula given by

$$u(r, T) = C_L \times u(r, T_L) + C_U \times u(r, T_U) \quad (17)$$

to determine the temperature dependent CG potentials for liquid n-hexane in a region of homogeneous phases. In Eq. (17), the CG potential at temperature  $T$ ,  $u(r, T)$ , is determined from the two known CG potentials  $u(r, T_L)$  and  $u(r, T_U)$  at temperatures  $T_L$  and  $T_U$ , where  $T_L \leq T \leq T_U$ , and  $C_L$  and  $C_U$  are the

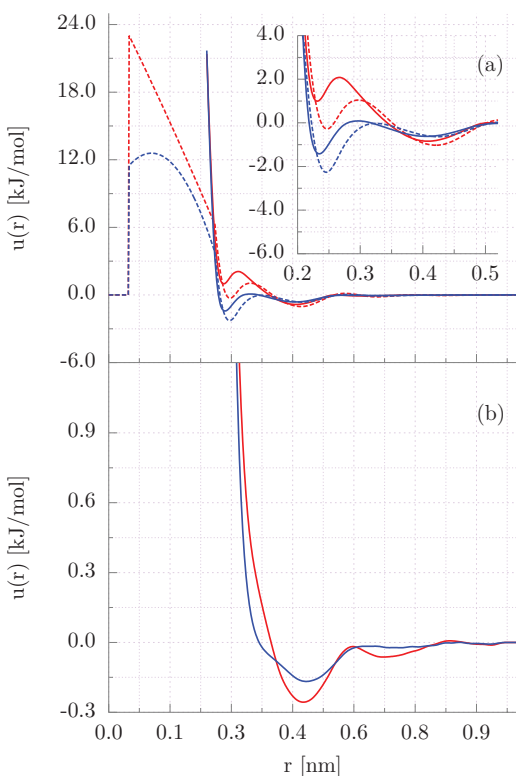


FIG. 3. Interpolated CG potentials for the confined water. The top subfigure shows water-water potentials where solid lines are CG-MD potentials and dashed lines are EQT potentials. The bottom subfigure shows carbon-water potentials. In both the subfigures, red lines are for  $T = 310$  K, and blue for  $T = 473$  K.

mixing coefficients given by

$$C_L = \frac{T_U - T}{T_U - T_L}, \quad (18a)$$

$$C_U = \frac{T - T_L}{T_U - T_L}. \quad (18b)$$

Herein, we test the applicability of 2-point linear interpolation formula for the confined water by evaluating the accuracy of the CG potentials derived for the saturated liquid water states:  $T = 310$  K,  $\rho = 0.9933$  gm/cm<sup>3</sup>, and  $T = 473$  K,  $\rho = 0.863$  gm/cm<sup>3</sup>. For  $T = 310$  K, we use  $T_L = 298$  K and  $T_U = 328$  K, and for  $T = 473$  K, we use  $T_L = 400$  K and  $T_U = 523$  K. The CG-MD and EQT potentials obtained by this procedure are shown in Fig. 3. From Fig. 4, it is evident that the density profiles of water predicted by the scaled CG-MD and EQT potentials are in reasonably good agreement with the reference AA-MD results. Therefore, it is clear that the 2-point linear interpolation can be used to derive state dependent CG potentials for the confined water in the region of the saturated liquid phases. We note that there is a scope to further investigate, in detail, the transferability of the CG potentials for the confined water in the region of much wider thermodynamic states using the relative entropy minimization and the PMF-matching techniques.

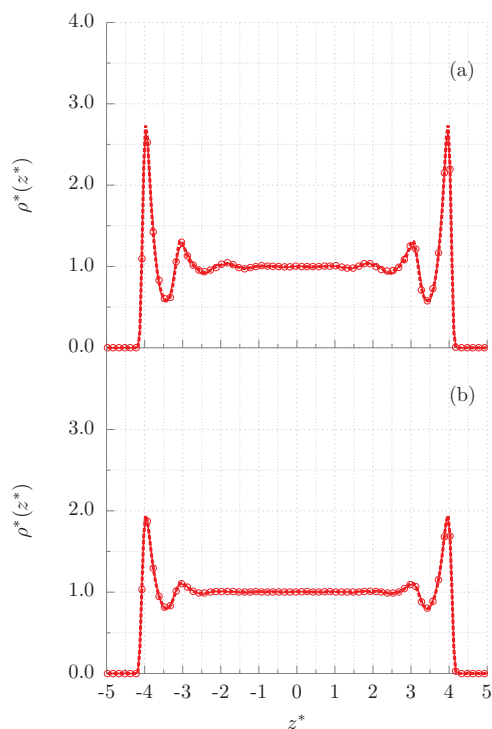


FIG. 4. Comparison of COM density profiles of water from AA-MD, CG-MD, and EQT simulations using interpolated CG potentials for  $10\sigma$  channel: (a)  $T = 310$  K and (b)  $T = 473$  K. In both the subfigures, circles are AA-MD results, solid lines are CG-MD results, and dashed lines are EQT results.  $z^*$  is defined as  $z/\sigma$  and  $\rho^* = \rho/\rho_{\text{bulk}}$ .

## V. CONCLUSIONS

In the present study, we demonstrated a systematic coarse-graining approach to optimize the structurally consistent carbon-water and water-water coarse-grained potentials for the graphene-water system. Two multiscale simulation approaches are demonstrated, namely the particle-based coarse-grained molecular dynamics (CG-MD) and the empirical potential-based quasi-continuum theory (EQT). It is found that the relative entropy based coarse-graining technique can be used to derive structurally consistent CG-MD potentials, which can be used in EQT to accurately predict the density profiles of the confined water. Both the carbon-water and water-water CG potentials are found to be significantly dependent on the thermodynamic state. However, for all the thermodynamic states studied, it is found that the water-water CG potential exhibits so-called core-softened double-well type characteristics, whose energy-scales are significantly state-dependent, whereas length-scales change very little. Also, it is shown that the 2-point linear interpolation formula can be useful to derive the CG potentials at thermodynamic states other than the one optimized here. Finally, we note that there is scope to further study, in detail, the scaling relations to derive the CG potentials for the confined water at wider thermodynamic states based on the optimized CG potentials at few representative states.

## ACKNOWLEDGMENTS

This work was supported by the NSF (Grant Nos. 0852657 and 0915718). S.Y.M. wishes to thank Christoph Junghans and Victor Rühle for their help with the VOTCA package. The authors acknowledge the use of the Taub cluster provided by the Computational Science and Engineering Program at the University of Illinois.

## APPENDIX A: RELATIVE ENTROPY MINIMIZATION

To minimize  $S_{\text{rel}}$  using the coupled Newton-Raphson scheme given by Eq. (9), we need to determine  $\nabla_{\lambda} S_{\text{rel}}$  and  $\mathbf{H}_{S_{\text{rel}}}$ .  $\nabla_{\lambda} S_{\text{rel}}$  can be computed as

$$\nabla_{\lambda} S_{\text{rel}} = \beta \left\langle \frac{\partial U_{\text{CG}}}{\partial \lambda} \right\rangle_{\text{AA}} - \beta \left\langle \frac{\partial U_{\text{CG}}}{\partial \lambda} \right\rangle_{\text{CG}}, \quad (\text{A1})$$

and  $\mathbf{H}_{S_{\text{rel}}}$  is given by

$$\begin{aligned} \mathbf{H}_{ij, S_{\text{rel}}} &= \beta \left\langle \frac{\partial^2 U_{\text{CG}}}{\partial \lambda_i \partial \lambda_j} \right\rangle_{\text{AA}} - \beta \left\langle \frac{\partial^2 U_{\text{CG}}}{\partial \lambda_i \partial \lambda_j} \right\rangle_{\text{CG}} \\ &+ \beta^2 \left\langle \frac{\partial U_{\text{CG}}}{\partial \lambda_i} \frac{\partial U_{\text{CG}}}{\partial \lambda_j} \right\rangle_{\text{CG}} \\ &- \beta^2 \left\langle \frac{\partial U_{\text{CG}}}{\partial \lambda_i} \right\rangle_{\text{CG}} \left\langle \frac{\partial U_{\text{CG}}}{\partial \lambda_j} \right\rangle_{\text{CG}}. \end{aligned} \quad (\text{A2})$$

Equations (A1) and (A2) require the average derivatives of the total CG potential energy in the AA-MD and CG-MD ensembles. To compute the averages in the AA-MD ensemble, a single well converged reference AA-MD simulation is performed and its AA configurations are saved, and then the average derivatives of the total CG potential energy are computed using the CG-MD pair potentials by processing the CG sites configurations in the AA-MD ensemble, which are obtained by mapping the reference AA sites configurations, as

$$\left\langle \frac{\partial U_{\text{CG}}}{\partial \lambda_i} \right\rangle_{\text{AA}} = \left\langle \sum_{m < n} \frac{\partial u_{\text{CG}}(r_{mn})}{\partial \lambda_i} \right\rangle_{\text{AA}}, \quad (\text{A3a})$$

$$\left\langle \frac{\partial^2 U_{\text{CG}}}{\partial \lambda_i \partial \lambda_j} \right\rangle_{\text{AA}} = \left\langle \sum_{m < n} \frac{\partial^2 u_{\text{CG}}(r_{mn})}{\partial \lambda_i \partial \lambda_j} \right\rangle_{\text{AA}}, \quad (\text{A3b})$$

where, the sum is performed over all the pairs  $(m, n)$  of the CG sites,  $u_{\text{CG}}(r)$  is replaced by  $u_{\text{CG}}^{\text{ww}}(r)$  when  $(m, n)$  is a water-water pair and by  $u_{\text{CG}}^{\text{cw}}(r)$  when  $(m, n)$  is a carbon-water pair. Both  $u_{\text{CG}}^{\text{ww}}(r)$  and  $u_{\text{CG}}^{\text{cw}}(r)$  are modeled by the SP potential form,  $u_{\text{SP}}(r)$ , and the first derivative of  $u_{\text{SP}}(r)$  with a knot value  $c_i$  can be determined from Eq. (4) as

$$\begin{aligned} \frac{\partial u_{\text{SP}}(r)}{\partial c_i} &= [1 \quad t \quad t^2 \quad t^3] \frac{1}{6} \begin{bmatrix} 1 & 4 & 1 & 0 \\ -3 & 0 & 3 & 0 \\ 3 & -6 & 3 & 0 \\ -1 & 3 & -3 & 1 \end{bmatrix} \\ &\times \begin{bmatrix} \delta_{i,j} \\ \delta_{i,j+1} \\ \delta_{i,j+2} \\ \delta_{i,j+3} \end{bmatrix}, \end{aligned} \quad (\text{A4})$$

where  $\delta$  is the Kronecker delta function such that  $\delta_{i,j} = 1$  if  $i = j$ , 0 otherwise. Because  $u_{\text{SP}}(r)$  is a linear function of  $c_i$ , its second derivatives with respect to  $c_i$  are zero. Since the CG-MD ensemble depends upon the CG-MD pair potential parameters, a short (about 500 ps long) CG-MD simulation is performed at each Newton-Raphson iteration step to generate corresponding CG-MD configurations and the averages in the CG-MD ensemble are computed in the similar manner as in Eq. (A3) by averaging over the CG-MD simulation configurations instead of the AA-MD configurations.

## APPENDIX B: PMF-MATCHING

In the PMF-matching technique, for the minimization of  $\epsilon_{\text{B}}$  using Eq. (16), we need to determine  $\nabla_{\lambda} \epsilon_{\text{B}}$  and  $\mathbf{H}_{\epsilon_{\text{B}}}$ .  $\nabla_{\lambda} \epsilon_{\text{B}}$  can be computed from Eq. (15) as

$$\begin{aligned} \nabla_{\lambda} \epsilon_{\text{B}} &= -\frac{1}{L} \int_0^L \frac{1}{RT} \rho_0^{\text{tgt}} \exp\left(-\frac{\bar{U}(z)}{RT}\right) \\ &\times \left( \rho_0^{\text{tgt}} \exp\left(-\frac{\bar{U}(z)}{RT}\right) - \rho^{\text{tgt}}(z) \right) \frac{\partial \bar{U}(z)}{\partial \lambda} dz, \end{aligned} \quad (\text{B1})$$

and  $\mathbf{H}_{\epsilon_{\text{B}}}$  is given by

$$\begin{aligned} \mathbf{H}_{ij, \epsilon_{\text{B}}} &= \frac{1}{L} \int_0^L \left( \frac{1}{RT} \right)^2 \rho_0^{\text{tgt}} \exp\left(-\frac{\bar{U}(z)}{RT}\right) \\ &\times \left( \rho_0^{\text{tgt}} \exp\left(-\frac{\bar{U}(z)}{RT}\right) - \rho^{\text{tgt}}(z) \right) \frac{\partial \bar{U}(z)}{\partial \lambda_i} \frac{\partial \bar{U}(z)}{\partial \lambda_j} dz \\ &+ \frac{1}{L} \int_0^L \left( \frac{1}{RT} \rho_0^{\text{tgt}} \exp\left(-\frac{\bar{U}(z)}{RT}\right) \right)^2 \frac{\partial \bar{U}(z)}{\partial \lambda_i} \frac{\partial \bar{U}(z)}{\partial \lambda_j} dz \\ &- \frac{1}{L} \int_0^L \frac{1}{RT} \rho_0^{\text{tgt}} \exp\left(-\frac{\bar{U}(z)}{RT}\right) \\ &\times \left( \rho_0^{\text{tgt}} \exp\left(-\frac{\bar{U}(z)}{RT}\right) - \rho^{\text{tgt}}(z) \right) \frac{\partial^2 \bar{U}(z)}{\partial \lambda_i \partial \lambda_j} dz. \end{aligned} \quad (\text{B2})$$

Since  $\lambda$  in Eq. (16) contains only the parameters of the water-water pair potential,  $u_{\text{EQT}}^{\text{ww}}(r)$ , only the water-water potential profile  $U^{\text{ww}}(z)$  contributes to the first and second derivatives of  $\bar{U}(z)$  in Eqs. (B1) and (B2), and they can be computed as

$$\frac{\partial \bar{U}(z)}{\partial \lambda_i} = \frac{\partial U^{\text{ww}}(z)}{\partial \lambda_i} - \frac{\partial U^{\text{ww}}(z_0)}{\partial \lambda_i}, \quad (\text{B3a})$$

$$\frac{\partial^2 \bar{U}(z)}{\partial \lambda_i \partial \lambda_j} = \frac{\partial^2 U^{\text{ww}}(z)}{\partial \lambda_i \partial \lambda_j} - \frac{\partial^2 U^{\text{ww}}(z_0)}{\partial \lambda_i \partial \lambda_j}, \quad (\text{B3b})$$

where  $\frac{\partial U^{\text{ww}}}{\partial \lambda_i}$  and  $\frac{\partial^2 U^{\text{ww}}}{\partial \lambda_i \partial \lambda_j}$  are given by

$$\frac{\partial U^{\text{ww}}(r)}{\partial \lambda_i} = \int \rho(r') \frac{\partial u_{\text{EQT}}^{\text{ww}}(|r-r'|)}{\partial \lambda_i} dr', \quad (\text{B4a})$$

$$\frac{\partial^2 U^{\text{ww}}(r)}{\partial \lambda_i \partial \lambda_j} = \int \rho(r') \frac{\partial^2 u_{\text{EQT}}^{\text{ww}}(|r-r'|)}{\partial \lambda_i \partial \lambda_j} dr'. \quad (\text{B4b})$$

The first derivatives of  $u_{\text{EQT}}^{\text{ww}}(r)$  with respect to  $a_1$  and  $a_2$  can be computed from Eq. (12) as

$$\frac{\partial u_{\text{EQT}}^{\text{ww}}(r)}{\partial a_1} = r - R_{\min}, \quad (\text{B5a})$$

$$\frac{\partial u_{\text{EQT}}^{\text{ww}}(r)}{\partial a_2} = (r - R_{\min})^2, \quad (\text{B5b})$$

and the first derivatives with respect to the knot values of the B-spline part of  $u_{\text{EQT}}^{\text{ww}}(r)$  can be computed by Eq. (A4). The second derivatives of  $u_{\text{EQT}}^{\text{ww}}(r)$  with respect to  $\lambda$  are zero. For the graphene-water slit-like system, we follow the same procedure described in the Appendix of Ref. 11 to determine  $U(z)$ ,  $U^{\text{cw}}(z)$ ,  $U^{\text{ww}}(z)$ , and the derivatives of  $U(z)$ .

<sup>1</sup>M. F. Chaplin, in *Adsorption and Phase Behaviour in Nanochannels and Nanotubes*, edited by L. J. Dunne, and G. Manos (Springer, Netherlands, 2010), pp. 241–255.

<sup>2</sup>J. C. Rasaiah, S. Garde, and G. Hummer, *Annu. Rev. Phys. Chem.* **59**, 713 (2008).

<sup>3</sup>R. Qiao and N. R. Aluru, *J. Chem. Phys.* **118**, 4692 (2003).

<sup>4</sup>S. Attinger and P. Koumoutsakos, *Multiscale Modeling and Simulation* (Springer, New York, 2004).

<sup>5</sup>F. Müller-Plathe, *ChemPhysChem* **3**, 755 (2002).

<sup>6</sup>C. Peter and K. Kremer, *Soft Matter* **5**, 4357 (2009).

<sup>7</sup>W. L. Jorgensen and J. Tirado-Rives, *Proc. Natl. Acad. Sci. U.S.A.* **102**, 6665 (2005).

<sup>8</sup>A. Wallqvist and R. D. Mountaint, *Reviews in Computational Chemistry* (Wiley, 2007), Vol. 13, Chap. 4, pp. 183–247.

<sup>9</sup>H. J. C. Berendsen, J. R. Grigera, and T. P. Straatsma, *J. Phys. Chem.* **91**, 6269 (1987).

<sup>10</sup>A. V. Raghunathan, J. H. Park, and N. R. Aluru, *J. Chem. Phys.* **127**, 174701 (2007).

<sup>11</sup>S. Y. Mashayak and N. R. Aluru, *J. Chem. Theory Comput.* **8**, 1828 (2012).

<sup>12</sup>V. Rühle, C. Junghans, A. Lukyanov, K. Kremer, and D. Andrienko, *J. Chem. Theory Comput.* **5**, 3211 (2009).

<sup>13</sup>S. Izvekov and G. A. Voth, *J. Chem. Phys.* **123**, 134105 (2005).

<sup>14</sup>A. Chaimovich and M. S. Shell, *Phys. Chem. Chem. Phys.* **11**, 1901 (2009).

<sup>15</sup>H. Wang, C. Junghans, and K. Kremer, *Eur. Phys. J. E* **28**, 221 (2009).

<sup>16</sup>A. A. Louis, *J. Phys.: Condens. Matter* **14**, 9187 (2002).

<sup>17</sup>M. E. Johnson, T. Head-Gordon, and A. A. Louis, *J. Chem. Phys.* **126**, 144509 (2007).

<sup>18</sup>J. Martí, J. Sala, and E. Guàrdia, *J. Mol. Liq.* **153**, 72 (2010).

<sup>19</sup>S. K. Das, M. M. Sharma, and R. S. Schechter, *J. Phys. Chem.* **100**, 7122 (1996).

<sup>20</sup>A. Ghoufi, D. Morineau, R. Lefort, I. Hureau, L. Hennou, H. Zhu, A. Szymczyk, P. Malfreyt, and G. Maurin, *J. Chem. Phys.* **134**, 074104 (2011).

<sup>21</sup>E. Schmidt, *Properties of Water and Steam in SI Units* (Springer-Verlag, Düsseldorf, 1969).

<sup>22</sup>B. Hess, C. Kutzner, D. van der Spoel, and E. Lindahl, *J. Chem. Theory Comput.* **4**, 435 (2008).

<sup>23</sup>T. Darden, D. York, and L. Pedersen, *J. Chem. Phys.* **98**, 10089 (1993).

<sup>24</sup>S. Nosé, *J. Chem. Phys.* **81**, 511 (1984).

<sup>25</sup>M. S. Shell, *J. Chem. Phys.* **129**, 144108 (2008).

<sup>26</sup>D. Wu and D. A. Kofke, *J. Chem. Phys.* **123**, 054103 (2005).

<sup>27</sup>A. Chaimovich and M. S. Shell, *J. Chem. Phys.* **134**, 094112 (2011).

<sup>28</sup>A. Chaimovich and M. Shell, *Phys. Rev. E* **81**, 060104 (2010).

<sup>29</sup>T. Sanghi and N. R. Aluru, *J. Chem. Phys.* **132**, 044703 (2010).

<sup>30</sup>T. Sanghi and N. R. Aluru, *J. Chem. Phys.* **136**, 024102 (2012).

<sup>31</sup>See supplementary material at <http://dx.doi.org/10.1063/1.4769297> for the coarse-grained potential parameters of the coarse-grained molecular dynamic simulation method and the coarse-grained potential parameters of the empirical potential-based quasi-continuum theory simulation method.

<sup>32</sup>Z. Yan, S. V. Buldyrev, N. Giovambattista, P. G. Debenedetti, and H. E. Stanley, *Phys. Rev. E* **73**, 051204 (2006).

<sup>33</sup>Z. Yan, S. V. Buldyrev, P. Kumar, N. Giovambattista, and H. E. Stanley, *Phys. Rev. E* **77**, 042201 (2008).

<sup>34</sup>E. Velasco and P. Tarazona, *J. Chem. Phys.* **91**, 7916 (1989).

<sup>35</sup>K. Farah, A. C. Fogarty, M. C. Böhm, and F. Müller-Plathe, *Phys. Chem. Chem. Phys.* **13**, 2894 (2011).